Surface segregation of interstitial manganese in $Ga_{1-x}Mn_xAs$ studied by hard x-ray photoemission spectroscopy

B. Schmid,* A. Müller, M. Sing, and R. Claessen
Experimentelle Physik IV, Physikalisches Institut, Universität Würzburg, Am Hubland, 97072 Würzburg, Germany

J. Wenisch, C. Gould, K. Brunner, and L. Molenkamp
Experimentelle Physik III, Physikalisches Institut, Universität Würzburg, Am Hubland, 97072 Würzburg, Germany

W. Drube
Deutsches Elektronen-Synchrotron (DESY), Notkestrasse 85, 22603 Hamburg, Germany
(Received 19 December 2007; revised manuscript received 3 July 2008; published 22 August 2008)

The effects of low-temperature annealing and oxidation of the dilute magnetic semiconductor $Ga_{1-x}Mn_xAs$ are studied by photoemission spectroscopy in the hard x-ray regime (HAXPES), with special attention to the depth profile of both concentration and chemical state of manganese. Annealing of $Ga_{1-x}Mn_xAs$ in air at 190 °C for up to 150 h leads to an enrichment of manganese at the surface accompanied by an increase in the native oxide layer. These observations are consistently explained by thermally activated surface segregation of interstitial Mn and its subsequent passivation by oxidation, thereby confirming a recently suggested mechanism for an enhancement of the Curie temperature upon annealing.

DOI: 10.1103/PhysRevB.78.075319 PACS number(s): 75.50.Pp, 79.60.Bm, 81.40.−z, 81.65.Mq

I. INTRODUCTION

Utilizing the electronic spin as information carrier opens up new perspectives for electronic data processing and storage. A prime goal in spintronics is an easier combination or even unification of semiconductor-based processing units and magnetic storage components.[1] This requires novel device concepts and suitable materials for alignment and injection of spin-polarized currents into integrated circuits. Despite the physical obstacles set by the basic incompatibility of conventional semiconductors and ferromagnetic materials large progress has been made in this field within the last decade. In this context dilute magnetic semiconductors (DMS) based on III-V compounds, especially Mn-doped GaAs, have raised tremendous interest because they combine ferromagnetism with conventional semiconductor technology within the same material. Since its first epitaxial growth in 1996 by Ohno and co-workers[2] many research activities were focused on $Ga_{1-x}Mn_xAs$ with x in the range 1%–8%, which displays ferromagnetism at low temperatures. While the ferromagnetism in (Ga,Mn)As is known to be mediated by a Ruderman-Kittel-Kasuya-Yosida (RKKY)-type interaction between the Mn atoms[3] a lot of effort has been spent in order to empirically optimize the material for spintronics applications. The key property here is the Curie temperature T_c, which initially was rather low (below 75 K)[2] but has since been increased to values as high as 180 K.[4]

A key issue in the optimization of the magnetic properties of $Ga_{1-x}Mn_xAs$ is the thermal treatment after molecular beam epitaxy. It was observed that annealing in air at moderate temperatures (190 °C) for relatively long periods of time (>100 h) enhances the Curie temperature as well as the magnetic remanence and the electric conductivity.[5,6] This has been suggested to be related to a selective removal of defects and is imagined as follows. In order to avoid complete surface segregation of Mn and the formation of MnAs clusters, $Ga_{1-x}Mn_xAs$ thin films are grown at comparably low temperatures (below 270 °C) on a GaAs substrate, resulting in a significant amount of various defects. A previous study[7] showed that the contribution of arsenic antisites [known to be the major defect in LT-grown GaAs[8]] is only important at very low Mn concentrations. Hence, the magnetic and transport properties are essentially determined by the manganese impurities, which can be distinguished into substitutional and interstitial Mn. The ferromagnetism is believed,[9] supported by numerous experiments, to be mediated by holes provided by substitutional Mn on Ga sites which acts as single acceptor, i.e., supplies one hole per Mn ion. In contrast, interstitial Mn is a double donor meaning that in principle one interstitial Mn compensates two substitutional Mn, thereby adversely affecting transport and magnetism. It is widely believed that annealing in air provides enough activation energy for interstitial manganese to segregate at the surface and be passivated by oxidation, whereas the Mn on Ga sites remains widely unaffected.[6] However, this model has been questioned.[10] The annealing process is very sensitive to both duration and temperature, and can also lead to other diffusion effects like the formation of antiferromagnetically ordered Mn-Mn clusters, especially at high Mn concentration.[11]

Annealing effects in $Ga_{1-x}Mn_xAs$ have been studied by various techniques. Channeling Rutherford backscattering (c-RBS) and channeling particle induced x-ray emission (c-PIXE),[12] x-ray absorption in magnetic circular dichroism[13] and Auger electron spectroscopy[6] have been applied as well as theoretical studies using first-principles Monte Carlo simulations.[14,15] The present paper utilizes the chemical state information obtained by hard x-ray photoelectron spectroscopy (HAXPES) for a systematic study of long-term low-temperature annealing. The results provide detailed information on the chemical depth profile and the oxidation processes, with particular focus on the annealing time depen-

dence. They confirm the above picture and give additional insight into the mechanisms underlying the annealing-induced T_c optimization of $Ga_{1-x}Mn_xAs$.

II. EXPERIMENT

$Ga_{1-x}Mn_xAs$ thin films with a nominal Mn concentration of 5%–6% and a thickness of 60 nm were grown on a GaAs substrate by low-temperature molecular beam epitaxy (LT-MBE) at 270 °C.[16] The films were thermally treated in air at 190 °C for various periods of time in order to obtain snapshots of the chemical composition and chemical states during the segregation process. For reference we also took data on a bulk MnAs sample, whose surface was cleaned by *in situ* filing, thus providing an oxide-free and hence intrinsic signal.

The HAXPES experiments have been performed at beamline BW2 of HASYLAB, DESY in Hamburg, Germany, using a SCIENTA SES-200 electron spectrometer optimized for photoemission in the hard x-ray regime.[17] By choosing the excitation energy in the hard x-ray region (>2 keV) the probed depth can be as large as 15 nm or even larger due to the higher kinetic energy of the photoelectrons.[18] The data presented here were taken with an excitation energy of $h\nu$ =4.5 keV and an overall energy resolution of 0.7 eV. All spectra shown are calibrated to the position of the $4f_{7/2}$ (binding energy 83.9 eV) signal of a Au foil in electric contact to the sample.

Core-level photoemission not only provides information on the elemental composition of a solid, but also allows to identify the different chemical states of the elements by their respective binding energy shifts. In our study we utilized this effect to distinguish between oxidized and nonoxidized species. Moreover, angle-dependent photoemission allows a quantitative determination of the surface oxide layer thickness, assuming a reasonably sharp interface between the oxide and the intrinsic bulk.[19] If both the elemental density and the inelastic mean free path (IMFP) of the photoelectrons are identical in the substrate and the oxide, the overlayer thickness d_{ox} is given by

$$d_{ox} = \lambda \ln\left(\frac{I_{ox}}{I_{bulk}} + 1\right)\cos\alpha, \qquad (1)$$

where I_{bulk} and I_{ox} are the measured intensities of the bulk and oxidized species of the same element, respectively, as obtained from a Voigt profile fit of the core spectra. The emission angle α is defined relative to the surface normal, and the IMFP λ has been taken from Ref. 20. It has been shown that this technique provides reliable values for the oxide layer thickness on GaAs.[21]

An analysis of the stoichiometry is obtained from the core-level intensities. Taking into account the photoionization cross section, IMPF (which depends on the kinetic energy of the photoelectrons), the asymmetry factors of the orbitals, the transmission function of the analyzer, and the experimental geometry the relative concentrations of the chemical constituents in a sample can be obtained.[19] However, all these factors are affected by an error. Especially a large uncertainty arises from the photoionization cross sections, which are only calculated for the free atoms.[22] The IMPF and the transmission function can be controlled by using a reference system with known composition (in our case MnAs). For example, for our MnAs sample we would thus obtain a Mn-to-As ratio of 0.56 from the measured Mn $2p_{3/2}$ and As $2p_{3/2}$ intensities, whereas its real composition is known to be close to the nominal one.[23] We utilized these reference data (which was fairly constant for a wide range of detection angles, indicating that photodiffraction effects can be neglected) for a recalibration of the relative cross sections, allowing us to determine precise Mn concentrations from our $Ga_{1-x}Mn_xAs$ spectra. Only the background subtraction for each core level and the integrated intensity are still sources of error. Varying both procedures for all relevant lines leaves us with an error bar of approximately 10% for all stoichiometric analysis.

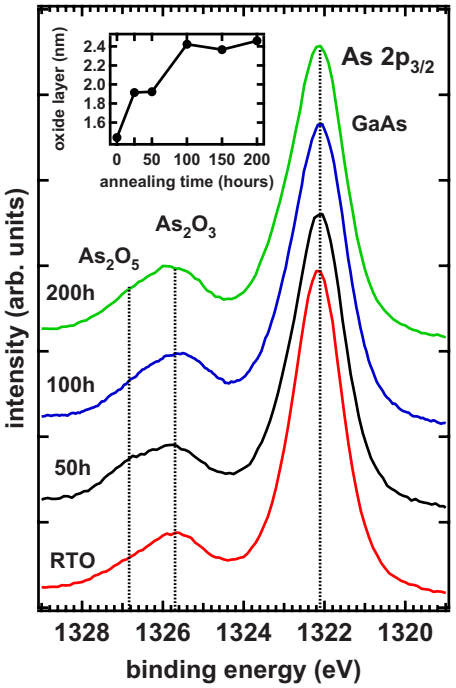

FIG. 1. (Color online) Evolution of the As $2p_{3/2}$ core-level spectra of a RTO sample as function of annealing time at 190 °C recorded in normal emission geometry. The oxide-related peaks gain intensity at the expense of the intrinsic peak. Inset: Oxide layer thickness as obtained from the spectra and Eq. (1). The native oxide thickness of 1.4 nm increases up to 2.4 nm upon annealing and saturates at this value.

III. RESULTS

Figure 1 shows the spectrum of the As $2p_{3/2}$ level as function of annealing time. It consists of two features, with the peak at 1322.2 eV corresponding to the intrinsic As species, while the broad side peak at higher binding energy (BE) results from oxidized As at the surface. The term "intrinsic" refers here to As bound to Ga. The different energy shift of As bound to Ga and bound to Mn is too small to be resolved. Furthermore, since only one out of ten As is stoichiometrically bound to Mn the As main peak is dominated by the

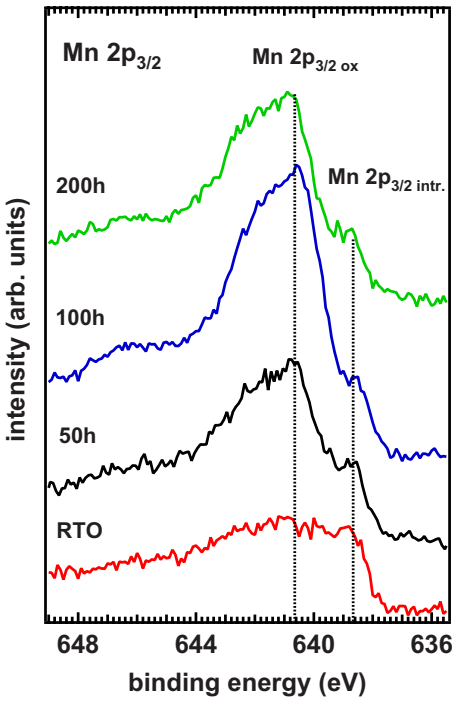

FIG. 2. (Color online) Evolution of Mn $2p_{3/2}$ core-level spectra recorded in normal emission geometry on a RTO sample as function of annealing time at 190 °C. The oxide-related Mn component increases at the expense of the intrinsic Mn peak of $Ga_{0.95}Mn_{0.05}As$.

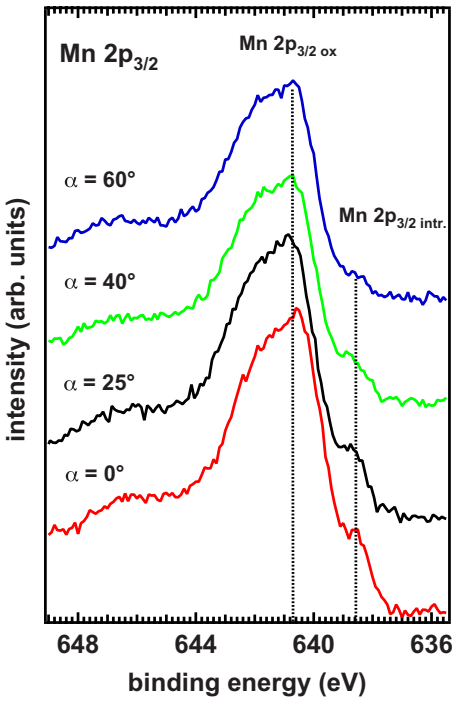

FIG. 3. (Color online) Angle-dependent Mn $2p_{3/2}$ core-level spectra of a $Ga_{0.95}Mn_{0.05}As$ sample annealed for 100 h at 190 °C. The low-binding energy shoulder at ≈638.6 eV increases with the probed depth. For each annealing time as well as the not-annealed sample a similar behavior is observed.

signal from As bound to Ga. The main oxide component is As_2O_3 with a chemical shift of 3.6 eV in good agreement to a value of 3.2 eV in the literature.[21] The high BE tail of the oxide peak is attributed to higher oxidation states such as As_2O_5. For the further analysis of the spectra the intensities have been decomposed into the intrinsic and an integral oxide contribution.

At first glance the relative oxide weight does not seem to depend strongly on annealing time. However, a closer inspection reveals that the integrated intensity of the oxide peak grows slightly at the expense of the intrinsic As signal. The same behavior is observed in the Ga $2p_{3/2}$ spectrum (not shown here). These data allow a quantitative determination of the surface oxide thickness using Eq. (1), the result of which is shown in the inset of Fig. 1. The graph reflects the evolution of the thickness as function of annealing time.[24,25] The untreated, i.e., room-temperature oxidized (RTO) sample gives an initial thickness of 1.4 nm which is only half as much as that reported by Allwood *et al.*[26] This discrepancy may originate from the uncertainty of the IMFP λ in Eq. (1). Figure 1 shows that the oxide layer thickness grows up to 2.4 nm with increasing annealing time and saturates at this value after ≈100 h. This oxide layer is however not to be confused with the surface layer mentioned by Kirby and co-workers,[27] since our calculation takes only the host matrix and their oxides into account. An additional surface layer consisting of Mn would only reduce the overall intensity and affects both the covalent and oxidized As peak.

A more pronounced oxidation effect is observed in the Mn $2p$ spectra, as displayed in Fig. 2. Like in Fig. 1 the data were recorded in normal emission geometry (α=0°), i.e., at highest volume sensitivity. Due to the low signal-to-noise ratio caused by the low Mn concentration (especially for the RTO sample) our discussion will focus on the Mn $2p_{3/2}$ spectrum. However, everything stated here also holds for Mn $2p_{1/2}$. In the case of the RTO sample the spectrum shows a broad double-peaked structure. Upon annealing in air, the feature on the high BE side strongly gains intensity while the low BE peak stays nearly constant.

Furthermore, after oxidation the Mn $2p$ spectrum displays a clear depth dependence. Figure 3 displays a series of spectra taken after 100 h annealing as function of electron escape angle, where the probing depth scales as $\lambda \cos(\alpha)$. The spectrum taken at α=60° thus probes only half as deep as the normal emission spectrum (0°) and therefore contains a much stronger surface contribution. Since the intensity of the low BE shoulder decreases with increasing surface sensitivity we attribute it to a Mn species in the bulk, whereas the intense high binding energy peak results from Mn atoms at or near the surface. In order to identify the valency of the various Mn species the data were compared to spectra of other Mn compounds. The low BE feature in our Mn $2p_{3/2}$ resembles strongly the spectrum of bulk MnAs (Fig. 4) and agrees with the XPS data on $Ga_{1-x}Mn_xAs$ by Okabayashi and co-workers.[28] We therefore attribute it to bulk Mn, with its low energy reflecting the covalent bonding to As. Despite the higher resolution compared to Ref. 28 we cannot distinguish between substitutional and interstitial Mn. In contrast, the high BE peak reflects a strongly oxidized Mn species.[29] Together with its angle dependence it can thus be assigned to a surface oxide. Our data are in contrast to an earlier report[30]

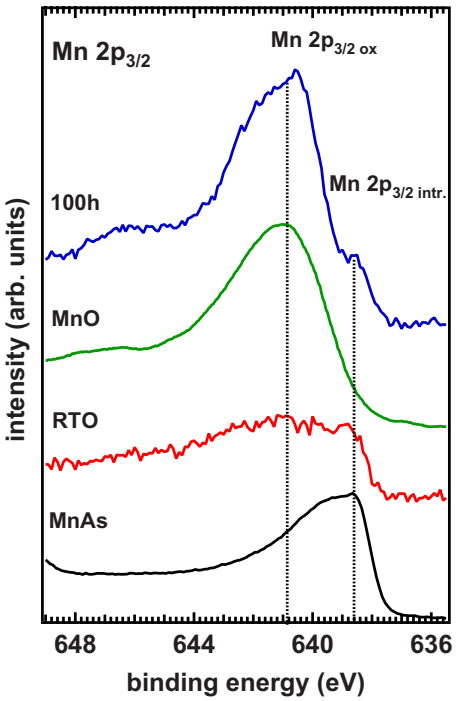

FIG. 4. (Color online) Comparison of the Mn $2p_{3/2}$ core-level spectra of $Ga_{1-x}Mn_xAs$ with reference data on MnAs and MnO (data taken from Ref. 29). All spectra are measured in normal emission geometry. For details see text.

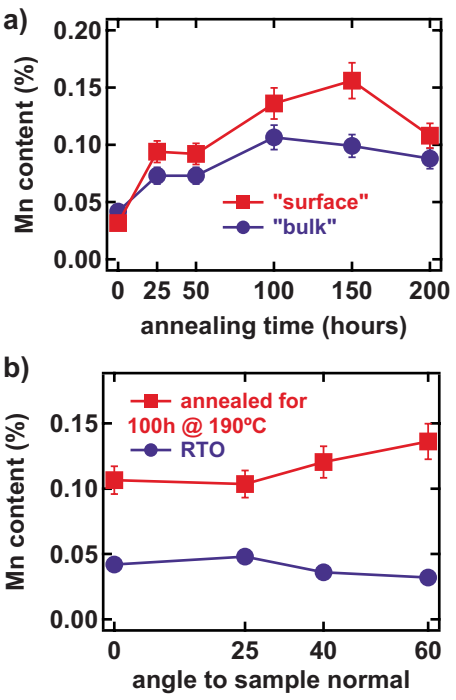

FIG. 5. (Color online) (a) Mn content as function of annealing time for two different probing depths ("bulk" and "surface" corresponding to emission angles of 0° and 60° with respect to the surface normal, respectively). (b) Mn content as a function of emission angle for not-annealed and 100 h annealed samples.

which ascribed the *high* BE feature to Mn covalently bound to As. However, our reference data on MnAs bulk samples show that the *low* BE feature is due to Mn bound to As, while the high BE feature has to be identified as an oxide component.

From the integrated Mn $2p$ signal we can also extract the quantitative stoichiometry within the probed sample volume. Figure 5(a) depicts the relative manganese content as function of annealing time as obtained for normal emission (highest bulk sensitivity) and $\alpha=60°$ (surface sensitive). The annealing temperature was kept low enough to avoid evaporation of As known from cleaning procedures on pure GaAs.[31] Figure 5(b) shows the angle dependence (and hence an effective depth profile) of the Mn content for the RTO and 100 h annealed sample. For the RTO sample the Mn content is 4.2%, slightly lower than the nominal content of 5%–6% obtained by x-ray diffraction (XRD)[16] after the MBE growth. From its angle independence we conclude on a homogeneous depth distribution. This is in clear contrast to the recent findings of Olejník *et al.*[4] who showed a significant increase in Mn signal toward the surface for as-grown samples. Though their samples were grown at even lower temperatures (200 °C) surface segregation seems to occur in their case whereas our samples show a homogeneous Mn distribution after growth. Upon annealing the situation changes significantly. The Mn content increases to 10.7% after 100 h and to even 15.6% at the surface after 150 h. It is apparent that the difference between bulk and surface concentration increases with annealing time. The depth profile of the annealed sample in Fig. 5(b) confirms a surface segregation of Mn. The slight decrease in the Mn surface content after 200 h annealing [Fig. 5(a)] may signal the onset of additional processes, which require further investigation.

IV. DISCUSSION

The increase in the overall surface oxide upon annealing as seen in Fig. 1 is intuitive. Progressive annealing and oxidation of the RTO sample increases the oxide layer thickness from 1.4 nm up to 2.4 nm. At this point the oxidation reaches saturation. A possible slight deviation of the absolute values from previous reports may be attributed to an uncertainty in the IMFP, but it does not affect the overall trend.

The most prominent annealing effect is however the increase in the Mn concentration by up to a factor of 4 in the surface-sensitive spectra and up to a factor of 2.5 in the normal emission data. Note that, while the latter is more bulk-sensitive, it still probes only the first 15 nm from the surface compared to an overall film thickness of 60 nm. More precisely, due to the enhanced but exponentially decreasing depth sensitivity the normal emission data are still affected by a non-negligible surface contribution. The overall angle (or depth) dependence of the annealed in contrast to the RTO sample in Fig. 5(b) can thus be well explained by a strong surface accumulation of Mn upon annealing. This can be explained by thermally activated segregation of Mn impurities to the surface and is further corroborated by the growing difference between surface and bulk Mn concentration with annealing time as seen in Fig. 5(a). From other experiments it is known that the oxidized Mn species at the surface can be removed completely by chemical etching,

while an intrinsic Mn bulk signal still remains.[32] This suggests that only one of the two intrinsic Mn species is subject to surface segregation. Spectroscopically we cannot distinguish between interstitial and substitutional Mn. However, the covalently bound Mn on substitutional sites has a higher activation energy than Mn on interstitial sites. Therefore we conclude that it is essentially interstitial Mn which accumulates at the surface upon annealing.

Another question concerns the passivation of Mn at the surface. In contrast to other PES[33] and x-ray absorption spectroscopy–magnetic circular dichroism (XAS-MCD) (Ref. 11) experiments, which investigated annealing effects of As-capped films in ultrahigh vacuum, our annealing was done under oxygen atmosphere. Therefore, the formation of MnAs as seen by Adell and co-workers[33] or a complex hybridization of different Mn species like in the data of Kronast *et al.*[11] is not observed. The surplus surface Mn is completely oxidized in our data.

We now turn to the identification of the oxidized species. The Mn $2p_{3/2}$ spectra of the RTO samples in Figs. 2 and 4 are composed of two different contributions. A comparison of the data to the spectra of other Mn compounds identifies the lower BE feature as similar to the Mn $2p_{3/2}$ spectrum of MnAs while the high BE peak has to be attributed to MnO. No clear evidence is seen for higher oxidation states such as in Mn_2O_3 or even MnO_2, which both would have a larger chemical shift relative to MnO by 0.5 eV and 1.0 eV, respectively. The low BE peak is interpreted as intrinsic Mn signal. Not only is the chemical environment of Mn in (Ga,Mn)As similar to that in MnAs, but it is precisely this peak which survives after chemical removal of the oxide layer by etching.[32] The increase in the MnO-related peak upon annealing shows that the segregated Mn is oxidized to Mn^{2+}.

In order to quantify the ratio of oxidized to intrinsic Mn integrated intensities of the various components have been determined by a fit routine. The contribution of the intrinsic covalently bound Mn was modeled by a single Voigt profile, whereas the oxide part was simulated by the sum of three Voigt profiles, accounting for multiple components and the charge transfer (CT) satellite of MnO around 646 eV.[29] The fit position, width, and relative intensity of the oxide-related peaks were fixed and only the intensity ratio of oxide to intrinsic peak was varied. The results are shown in Fig. 6 (the inset gives a fit example). For bulk-sensitive geometry the initial intrinsic-to-oxide ratio is 80%, whereas for the surface-sensitive spectra we find only 50%. The ratio decreases further for both experimental geometries with annealing time reaching a minimum after 150 h, with hardly any intrinsic signal left at the surface. This confirms the complete oxidation of the segregated interstitial Mn atoms.

Figure 7 shows the influence of the thermal treatment on the magnetic transition temperature and thereby correlates for one and the same sample the findings by HAXPES on Mn surface segregation and oxidation with the magnetic properties. In agreement with the literature,[6] T_c is significantly enhanced by annealing in air, for this sample from 64 K up to a maximum value of 118 K after 100 h annealing. By further annealing, T_c is slightly reduced, most likely due to the slow out-diffusion of Mn on substitutional sites which means a loss of magnetically active Mn, a reduction of the

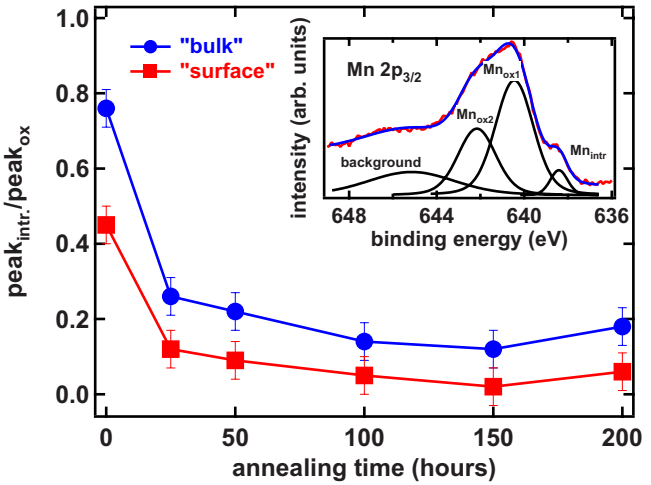

FIG. 6. (Color online) Intensity ratio of oxidized vs intrinsic Mn $2p_{3/2}$ components as function of annealing time for two different probing depths ("bulk" and "surface" corresponding to emission angles of 0° and 60° with respect to the surface normal, respectively). Inset: Example of decomposition of a Mn $2p_{3/2}$ spectrum into the various components. For details see text.

hole concentration, and hence a drop of T_c. The initial increase in the magnetic transition temperature occurs much faster than the increase in the Mn concentration in Fig. 5. This is simply due to the fact that superconducting quantum interference device (SQUID) measurements monitor an improvement of the magnetic response over the whole sample while the concomitant Mn diffusion appears in HAXPES only through an enhanced Mn concentration at the surface, i.e., with some delay. For the sake of completeness we note that the efficiency of the annealing depends on various factors such as temperature, film thickness—both kept constant in our study—or the oxide layer itself.[4,10,34] E.g., recently it was reported that a frequent removal of the oxide layer by etching during the annealing procedure[4] can lead to a further increase in T_c on a time scale 2 orders of magnitude shorter than in our case.

We thus arrive at the following picture. Thermal treatment of $Ga_{1-x}Mn_xAs$ causes interstitial Mn to diffuse to and accu-

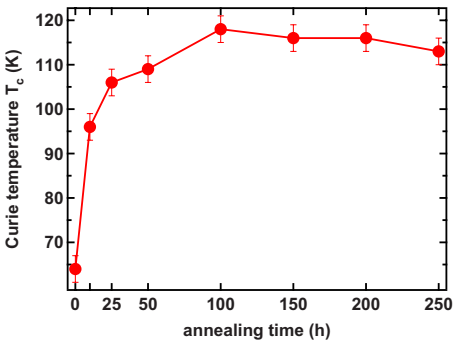

FIG. 7. (Color online) Curie temperature as a function of annealing time as derived from SQUID measurements. The increase by thermal treatment is clearly visible. It reaches a saturation value of 118 K after 100 h of annealing. This is followed by a slight decrease which is attributed to the out-diffusion of substitutional Mn.

mulate at the surface, while the substitutional acceptorlike Mn atoms remain largely unaffected. The annealing in air leads to a passivation of the segregated Mn atoms by oxidation, so they can no longer act as unwanted donors and compensate the hole carriers. These findings thus corroborate the suggested mechanism for an improvement of the Curie temperature by annealing in oxidizing atmosphere.

V. CONCLUSION

In summary, we have provided quantitative information on the segregation of Mn in $Ga_{1-x}Mn_xAs$. The amount of Mn at the surface increases by a factor of 4 while the overall oxide layer thickness grows by 60%. In contrast to the RTO sample, which shows a homogenous Mn distribution within the probing depth, the annealed samples show a clear Mn depth profile. Furthermore, the surplus Mn at the surface is passivated by oxidation to MnO. However, the loss of Mn for longer annealing times is not yet fully understood. Both the comparatively high activation energy as well as measurements on oxidized and subsequently etched samples exclude a major contribution of substitutional Mn to the segregation process. Our study also demonstrates the high potential of photoemission in the hard x-ray regime for the qualitative and quantitative analysis of *ex situ* prepared samples.

ACKNOWLEDGMENTS

The authors would like to thank H. Schulz-Ritter for the technical support. The MnAs samples were provided by H. Wada, Kyushu University, Fukuoka, Japan in cooperation with S. Imada, Osaka University, Osaka, Japan.

*schmid@physik.uni-wuerzburg.de

[1] G. A. Prinz, Science **282**, 1660 (1998).
[2] H. Ohno, A. Shen, F. Matsukura, A. Oiwa, A. Endo, S. Katsumoto, and Y. Ide, Appl. Phys. Lett. **69**, 363 (1996).
[3] T. Jungwirth, J. Sinova, J. Maek, J. Kuera, and A. H. MacDonald, Rev. Mod. Phys. **78**, 809 (2006).
[4] K. Olejník, M. H. S. Owen, V. Novak, J. Mašek, A. C. Irvine, J. Wunderlich, and T. Jungwirth, arXiv:0802.2080 (unpublished).
[5] K. C. Ku *et al.*, Appl. Phys. Lett. **82**, 2302 (2003).
[6] K. W. Edmonds *et al.*, Phys. Rev. Lett. **92**, 037201 (2004).
[7] R. C. Myers, B. L. Sheu, A. W. Jackson, A. C. Gossard, P. Schiffer, N. Samarth, and D. D. Awschalom, Phys. Rev. B **74**, 155203 (2006).
[8] X. Liu, A. Prasad, J. Nishio, E. R. Weber, Z. Liliental-Weber, and W. Walukiewicz, Appl. Phys. Lett. **67**, 279 (1995).
[9] T. Dietl, H. Ohno, F. Mastukura, J. Cibert, and D. Ferrand, Science **287**, 1019 (2000).
[10] M. Adell, J. Kanski, L. Ilver, J. Sadowski, V. Stanciu, and P. Svedlindh, Phys. Rev. Lett. **94**, 139701 (2005).
[11] F. Kronast *et al.*, Phys. Rev. B **74**, 235213 (2006).
[12] K. M. Yu, W. Walukiewicz, T. Wojtowicz, I. Kuryliszyn, X. Liu, Y. Sasaki, and J. K. Furdyna, Phys. Rev. B **65**, 201303(R) (2002).
[13] K. W. Edmonds, N. R. S. Farley, T. K. Johal, G. van der Laan, R. P. Campion, B. L. Gallagher, and C. T. Foxon, Phys. Rev. B **71**, 064418 (2005).
[14] H. Raebiger, M. Ganchenkova, and J. von Boehm, Appl. Phys. Lett. **89**, 012505 (2006).
[15] T. Hynninen, M. Ganchenkova, H. Raebiger, and J. von Boehm, Phys. Rev. B **74**, 195337 (2006).
[16] G. M. Schott, W. Faschinger, and L. W. Molenkamp, Appl. Phys. Lett. **79**, 1807 (2001).
[17] W. Drube, T. M. Grekh, R. Teusch, and G. Materlik, J. Electron Spectrosc. Relat. Phenom. **88-91**, 683 (1998).
[18] T. A. Carlson and G. E. McGuire, J. Electron Spectrosc. Relat. Phenom. **1**, 161 (1973).
[19] M. P. Seah, *Practical Surface Analysis*, 2nd ed. (Wiley, New York, 1990).
[20] S. Tanuma, C. J. Powell, and D. R. Penn, Surf. Interface Anal. **17**, 927 (1991).
[21] Z. Liu, Y. Sun, F. Machuca, P. Pianetta, W. E. Spicer, and R. F. W. Pease, J. Vac. Sci. Technol. A **21**, 212 (2003).
[22] M. B. Trzhaskovskaya, V. I. Nefedov, and V. G. Yarzhemsky, At. Data Nucl. Data Tables **77**, 97 (2001).
[23] H. Wada and Y. Tanabe, Appl. Phys. Lett. **79**, 3302 (2001).
[24] The plotted oxide thickness represents an average of the values determined from the As 2*p* and the Ga 2*p* spectrum, respectively. It is known that the Ga-derived surface oxide always comes out to be thicker than that of the As oxide, which has been explained by a chemically driven surface segregation of Ga during the oxidation process.
[25] J. T. Wolan, W. S. Epling, and G. B. Hoflund, J. Appl. Phys. **81**, 6160 (1997).
[26] D. A. Allwood, R. T. Carline, N. J. Mason, C. Pickering, B. K. Tanner, and P. J. Walker, Thin Solid Films **364**, 33 (2000).
[27] B. J. Kirby, J. A. Borchers, J. J. Rhyne, K. V. O'Donovan, S. G. E. te Velthuis, S. Roy, C. Sanchez-Hanke, T. Wojtowicz, X. Liu, W. L. Lim, M. Dobrowolska, and J. K. Furdyna, Phys. Rev. B **74**, 245304 (2006).
[28] J. Okabayashi, A. Kimura, O. Rader, T. Mizokawa, A. Fujimori, T. Hayashi, and M. Tanaka, Phys. Rev. B **58**, R4211 (1998).
[29] S.-P. Jeng, R. J. Lad, and V. E. Henrich, Phys. Rev. B **43**, 11971 (1991).
[30] S. Hatfield, T. Veal, C. McConville, G. Bell, K. Edmonds, R. Campion, C. Foxon, and B. Gallagher, Surf. Sci. **585**, 66 (2005).
[31] M. Yamada and Y. Ide, Surf. Sci. Lett. **339**, L914 (1995).
[32] B. Schmid, A. Müller, M. Sing, J. Wenisch, C. Gould, K. Brunner, L. W. Molenkamp, W. Drube, and R. Claessen (unpublished).
[33] M. Adell, J. Adell, L. Ilver, J. Kanski, J. Sadowski, and J. Z. Domagala, Phys. Rev. B **75**, 054415 (2007).
[34] K. W. Edmonds *et al.*, Phys. Rev. Lett. **94**, 139702 (2005).